Min-21 and Min-23, the Smallest Peptides That Fold Like a Cystine-Stabilized β-Sheet Motif: Design, Solution Structure, and Thermal Stability†

Annie Heitz,‡ Dung Le-Nguyen,§ and Laurent Chiche*,‡

Centre de Biochimie Structurale, Faculté de pharmacie, UMR9955 CNRS-INSERM-Université Montpellier I, 15 avenue Charles Flahault, 34060 Montpellier, France, and INSERM U376, CHU Arnaud-de-Villeneuve, 371 rue du doyen Gaston Giraud, 34295 Montpellier, France

Received April 8, 1999; Revised Manuscript Received June 3, 1999

ABSTRACT: Small disulfide-rich proteins provide examples of simple and stable scaffolds for design purposes. The cystine-stabilized β-sheet (CSB) motif is one such elementary structural motif and is found in many protein families with no evolutionary relationships. In this paper, we present NMR structural studies and stability measurements of two short peptides of 21 and 23 residues that correspond to the isolated CSB motif taken from a 28-residue squash trypsin inhibitor. The two peptides contain two disulfide bridges instead of three for the parent protein, but were shown to fold in a native-like fashion, indicating that the CSB motif can be considered an autonomous folding unit. The 23-residue peptide was truncated at the N-terminus. It has a well-defined conformation close to that of the parent squash inhibitor, and although less stable than the native protein, it still exhibits a high T_m of about 100 °C. We suggest that this peptide is a very good starting building block for engineering new bioactive molecules by grafting different active or recognition sites onto it. The 21-residue peptide was further shortened by removing two residues in the loop connecting the second and third cysteines. This peptide exhibited a less well-defined conformation and is less stable by about 1 kcal mol^{-1}, but it might be useful if a higher flexibility is desired. The lower stability of the 21-residue peptide is supposed to result from inadequate lengths of segments connecting the first three cysteines, thus providing new insights into the structural determinants of the CSB motif.

One attractive way to build new active molecules is to use a stable protein scaffold or a "mini-protein" as a framework on which to graft active sites or recognition fragments (*1*−*4*). Interestingly, small, stable, easy to synthesize scaffolds have been observed in small disulfide-rich proteins. In these proteins, the number of available structural motifs is probably very limited, and only very few different motifs are found in several proteins with very diverse origins and functions and with no apparent evolutionary relationship (*5*). This is consistent with the general fact that there are only a limited number of possible protein folds, and that similar folds can be observed in proteins with essentially no sequence identity (*6*−*8*). It is therefore important to identify and study such common scaffolds if one wants to use them in design strategy.

One such well-known motif is the CSH[1] (cystine-stabilized α-helical) motif (*5*, *9*, *10*) found in hormonal peptides from the endothelin family, apamin, scorpion toxins, insect defensins, plant γ-thionins, insectotoxins, and neurotoxins. The CSH motif is composed of a short helix linked to a short β-strand by two disulfide bridges (Figure 1A). Most structures, except the smallest ones (endothelin and apamin), are stabilized further by additional disulfide bridges. Another motif with three disulfide bridges, designated as the "inhibitor cystine knot motif" (*11*, *12*) or simply the "cystine motif" (*13*), has been found for the first time in the squash trypsin inhibitors (Figure 1B). These small disulfide-rich proteins (28−32 amino acids, six cysteines) are composed of a small triple-stranded β-sheet, one and one-half turns of a 3_{10}-helix, two β-turns, and the inhibitory loop (*14*). These secondary structural elements are organized around the three disulfide bridges that largely participate in the protein core. It was observed that one disulfide bridge crosses the macrocycle formed by the two other disulfide bridges and the interconnecting backbone, hence the term "cystine knot". Interestingly, the fold of the squash proteinase inhibitors was found to be strikingly similar to the fold of the carboxypeptidase inhibitor from potato PCI (*15*). It was subsequently shown that ω-agatoxins (*16*), ω-conotoxins (*17*, *18*), the race-specific elicitor Avr9 (*19*), gurmarin (*20*), huwentoxin-I (*21*), and the cyclic peptides kalata B1 (*22*) and circulin A (*23*) also share this structural motif (*11*, *13*). In these molecules, however, the 3_{10}-helix is not conserved but replaced by

† This work was supported by the Program Physique et Chimie du Vivant of the CNRS.

* To whom correspondence should be addressed. Telephone: +33 [0]4 67 04 34 32. Fax: +33 [0]4 67 52 96 23. E-mail: chiche@cbs.univ-montp1.fr.

‡ UMR9955 CNRS-INSERM-Université Montpellier I.

§ INSERM U376, CHU Arnaud-de-Villeneuve.

[1] Abbreviations: 1D, one-dimensional; 2D, two-dimensional; 3D, three-dimensional; CSB, cystine-stabilized β-sheet; CSH, cystine-stabilized α-helical; COSY, correlated spectroscopy; DQF, double-quantum-filtered; EETI II, *Ecballium elaterium* trypsin inhibitor II; NMR, nuclear magnetic resonance; NOE, nuclear Overhauser effect; H-bond, hydrogen bond; NOESY, nuclear Overhauser effect spectroscopy; PCI, potato carboxypeptidase inhibitor; rms, root-mean-square; TOCSY, total correlated spectroscopy.

10.1021/bi990821k CCC: $18.00
Published on Web 07/23/1999

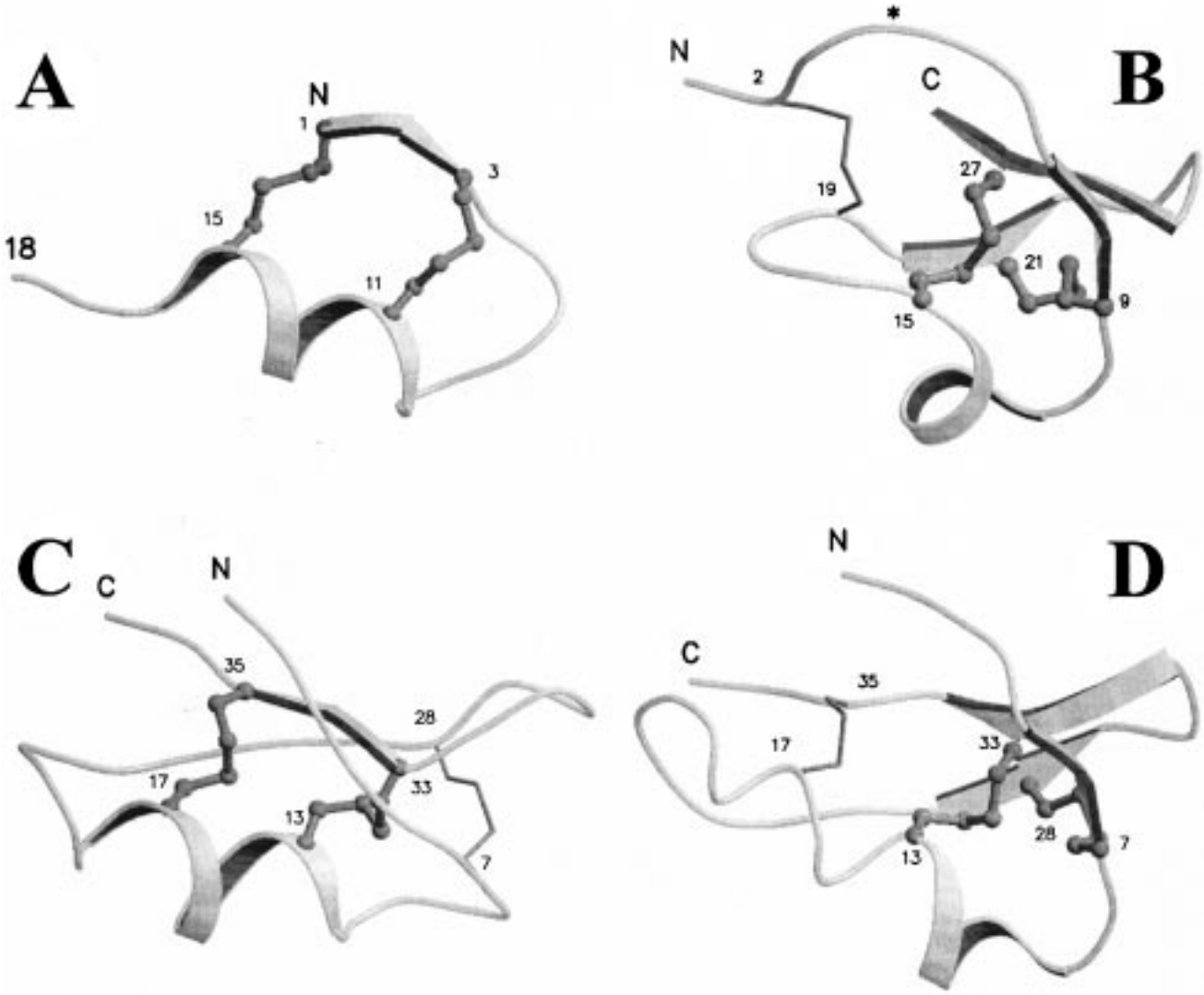

FIGURE 1: Schematic drawings of the two most common elementary disulfide bridge motifs: (A) the cystine-stabilized α-helical (CSH) motif in endothelin 1, (B) the cystine-stabilized β-sheet (CSB) motif in EETI II, (C) the CSH motif in charybdotoxin, and (D) the CSB motif in charybdotoxin. The N- and C-termini are labeled, and all cysteines are numbered. For convenience, the C-terminal tail in endothelin 1 is truncated at residue 18. The disulfide bridges participating in the displayed motifs are depicted as dark gray balls and sticks, whereas additional bridges are depicted as thin sticks. The location of the active site in EETI II is denoted by an asterisk in panel B. This figure was generated using the MOLSCRIPT (*45*) and RASTER3D (*46*) programs. Atom coordinates were taken from the Protein Data Bank (file names 2eti and 1crd) (*47*) and from ref *48* for endothelin 1.

variable loops. In contrast, the functional sites in these molecules are clearly different. The reactive site in the squash inhibitors is near the N-terminus, after the first cysteine (denoted by an asterisk in Figure 1B), whereas the reactive site in PCI is at the C-terminus. The neurotoxic activity of ω-agatoxins and ω-conotoxins is a result of their binding to N-type and P-type voltage-gated Ca^{2+} channels. The site of action of huwentoxin I is the postsynaptic nicotinic acetylcholine receptor. The active site of kalata B1 has not yet been identified, but it has been proposed that this peptide might contain a trypsin inhibitory site in the loop that links the N- and C-termini in other peptides (*11*). The mechanisms of action of gurmarin, a sweet-taste suppressing peptide, and of circulin A, an anti-HIV peptide, remain to be determined. Therefore, a second widespread motif, very distinct from the CSH motif, is present in proteins from different families with no known evolutionary relationships; this motif contains a triple-stranded β-sheet and three disulfide bridges forming a cystine knot.

However, we suggested that the strong structural similarity only concerned part of the molecules that includes two disulfide bridges and the small triple-stranded β-sheet (*15*). The fact that the essential motif contains only two disulfide bridges and constitutes an autonomous folding unit was further evidenced by its presence in a stable intermediate in the folding of EETI II, a 28-residue squash inhibitor (*24*). We propose to name this structural motif the CSB motif for cystine-stabilized β-sheet by analogy with the CSH motif, since the motif shown in Figure 1B is composed of a triple-stranded β-sheet stabilized by two disulfide bridges. It is worth noting that proteins exhibiting the CSB motif always include additional disulfides which are not strictly conserved, from a structural point of view. The arrangement of the disulfides in the CSB motif is also found in a number of larger proteins (*25*). It is also worth noting that combinations of the elementary disulfide-stabilized structural motifs have been used in nature to build more complex proteins, using a hierarchical topological organization. One nice example is

the scorpion toxin family that is a perfect combination of the CSH and the CSB motifs, as shown in panels C and D of Figure 1. This combination found in several protein families has been termed the cystine-stabilized $\alpha\beta$ motif (*26*).

Probably due to a particular stability, the CSB motif appears as one of the most widespread disulfide-rich motifs and is thus a priori highly tolerant to substitutions. It is a very appealing basic scaffold on which to graft active sites in the design of new active molecules. However, the elementary CSB motif alone has not yet been observed in nature; rather, it is always accompanied by complementary sequences and, at least, a third disulfide bridge. In this paper, we address the question of whether a short peptide containing only the CSB motif would be able to fold correctly and would be stable enough to constitute an interesting elementary disulfide-stabilized neutral scaffold for design purposes. One important point regarding the isolated CSB motif is that it is devoid of any active site, as is necessary for a basic scaffold for general use.

MATERIALS AND METHODS

NMR Spectroscopy. Peptides Min-21 and Min-23 were synthesized by Synt:em (Nimes, France) and purchased from them. The fully reduced peptides were oxidized in the presence of DMSO (*27*), and the major peak in HPLC was isolated. For the Min-23 peptide, the compound was used as is. For the Min-21 peptide, the HPLC peak was shown by NMR to contain two compounds in approximately equivalent quantities. However, one compound precipitated in a few hours after dissolution and could be removed by filtration. The remaining soluble compound was used for further work. Samples were prepared by dissolving peptides in H_2O (10% ^2H_2O) to a concentration of approximately 3−4 mM with the pH adjusted to 2.7 by addition of dilute HCl or NaOH.

All ^{1}H NMR spectra were recorded on 360, 400, or 600 MHz Bruker AMX spectrometers. Data were acquired at 12, 22, and 27 °C, and TSP-d_4 was used as an internal reference. All 2D experiments, DQF-COSY, TOCSY, and NOESY, were performed according to standard procedures (*49*) using quadrature detection in both dimensions with spectral widths of 10 ppm in both dimensions. The carrier frequency was centered on the water signal, and the solvent was suppressed by continuous low-power irradiation during the relaxation delay and during the mixing time for NOESY spectra. The 2D spectra were obtained using 2048 or 4096 points for each t_1 value, and 512 t_1 data points were acquired for TOCSY and NOESY experiments. Eight hundred t_1 increments were used for DQF-COSY. TOCSY spectra were recorded with spin lock times of 30 and 60 ms. The mixing times were 150 and 300 ms in NOESY spectra. All the results were zero filled to 1024 points in t_1 and multiplied by π/8- and π/4-shifted sine bell functions in the t_1 and t_2 domains, respectively, prior to Fourier transformation.

Exchange Experiments. The exchange of amide protons with deuterium was studied at 12 °C on 3−4 mM samples lyophilized from H_2O at pH 2.7 and dissolved in ^2H_2O. A series of 1D, TOCSY, and NOESY spectra were acquired over a 48 h period. The proton−deuterium exchange rates of the backbone amide protons were determined by following the residual intensities $I(t)$ of the NH peaks with time. The $\ln(k_{ex})$ for the exchange was obtained by fitting the data to a single exponential with Kaleidagraph (Synergy Software, Reading, PA):

$$I(t) = I_0 e^{-k_{ex}t}$$

Structure Calculations. All calculations were performed on a Silicon Graphics Origin 200 workstation. The structures were displayed and analyzed on a Silicon Graphics O2 workstation using the INSIGHT II program (MSI, San Diego, CA). The NOE intensities were classified as strong, medium, and weak, and converted into distance constraints of 2.5, 3, and 4 Å, respectively. If the connectivity involved side chain protons, 3.0, 4.0, and 5.0 Å upper bounds were used instead to account for higher mobility. For sequential $d_{\alpha N}$ and d_{NN} connectivities, we used bounds of 2.5, 3.0, and 3.5 Å and 2.8, 3.3, and 4.0 Å. When necessary, the distance constraints were corrected for pseudoatoms according to Wüthrich et al. (*50*). Φ angles of residues with small or large $^3J_{HN-H\alpha}$ coupling constants (<4 or >8.5 Hz) were constrained in the −90 to −40° or −160 to −80° ranges. χ_1 angles of residues for which stereospecific attribution of the β-protons could be achieved were constrained in the corresponding range. Disulfide bridges were imposed through distance constraints of 2.0−2.1, 3.0−3.1, and 3.75−3.95 Å on S_i-S_j, $S_i-C\beta_j$, $S_j-C\beta_i$, and $C\beta_i-C\beta_j$ distances, respectively. No H-bonds were imposed.

3D structures were obtained from the distance and angle restraints using the torsion angle molecular dynamics method available in the DYANA program (*28*). Eight hundred structures were calculated with the standard simulated annealing protocol for each of the three possible disulfide connectivities. In each case, the 20 structures with the lowest violation of the target function were selected for further refinement. These were submitted to molecular mechanics energy refinement with the SANDER module of the AMBER program (*29*), using the parm94 force field (*30*). To reduce well-known artifacts arising from in vacuo simulations (charged and polar side chains tend to fold back toward the protein to find an H-bonding partner), the net charge of ionized side chains was reduced to ±0.2 and a distance-dependent dielectric constant was used [$\epsilon = r$ (*31*)]. During the molecular dynamics runs, the covalent bond lengths were kept constant by applying the SHAKE algorithm (*32*), allowing a 1.5 fs time step to be used. The nonbonded pair list was updated every 20 steps, and the temperature was regulated by coupling the system to a heat bath with a coupling constant of 0.2 ps. Pseudoenergy terms taking into account the NMR interproton distance restraints were defined as follows via four threshold distance values: r_1-r_4. In all cases, r_1 and r_2 were set to 1.3 and 1.8 Å, respectively. r_3 was taken as the upper boundary used in the DYANA calculations, and r_4 was chosen as $r_3 + 0.5$ Å. For an observed distance lying between r_2 and r_3, no restraint was applied. Between r_1 and r_2 or between r_3 and r_4, parabolic restraints were applied. Outside the r_1-r_4 range, the restraints were linear with slopes that were identical at parabolic slopes at points r_1 and r_4. A similar strategy was used for dihedral restraints. When no stereospecific assignment could be achieved for methyl or methylene protons, an $(r^{-6})^{-1/6}$ averaging scheme was used instead of pseudoatoms. Five

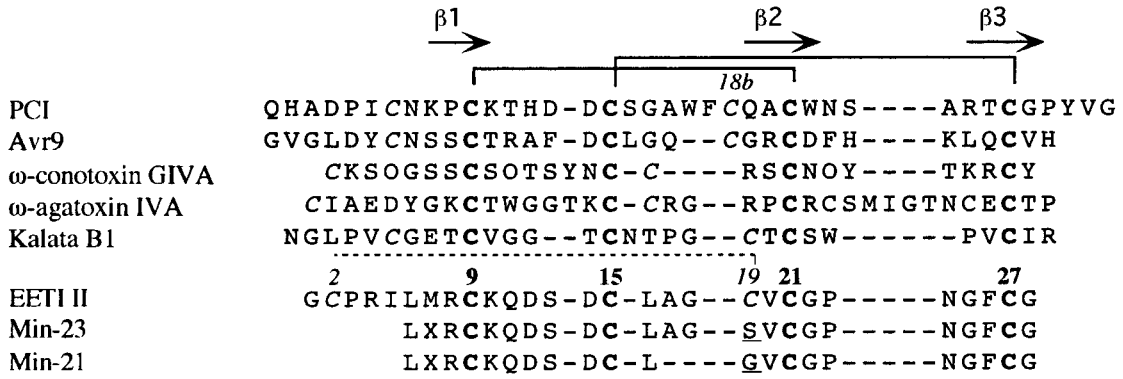

FIGURE 2: Sequence alignment of peptides Min-21 and Min-23 with small proteins containing the cystine-stabilized β-sheet motif. The alignment is based on structural superimposition of the motif, and the numbering is from EETI II (superimposed residues are 7−9, 14 and 15, 19−22, and 26−28; note that cysteines 9, 15, 21, and 27 form the two disulfide bridges present in the CSB motif). The two disulfide bridges of the CSB motif are depicted as black lines and bold cysteines. The third disulfide bridge in EETI II is depicted as dashed lines and cysteines in italics. The corresponding third bridge in PCI and Avr9 (Cys^5−Cys^{18b}), in conotoxin (Cys^2−Cys^{16}), in agatoxin (Cys^1−Cys^{16}), and in Kalata (Cys^5−Cys^{19}) is only denoted by cysteines in italics. The additional fourth bridge in agatoxin (Cys^{23}−Cys^{25}) is not depicted. The positions of the β-strands are denoted by arrows on top of the sequences. 4-Hydroxyprolines and norleucines are represented by the letters O and X, respectively. The mutated residues at position 19 in Min-21 and Min-23 are underscored. Sequences were taken from the Protein Data Bank (file names 2eti, 4cpa, 1omc, 1iva, and 1kal) (*47*) and from ref *19* for Avr9 elicitor.

thousand cycles of restrained energy minimization were first carried out followed by a 30 ps long simulated annealing procedure in which the temperature was raised to 900 K for 20 ps and then gradually lowered to 300 K. During this stage, the force constant for the NMR distance and dihedral constraints was gradually increased from 3.2 to 32 kcal mol^{-1} $Å^{-2}$ and from 0.5 to 50 kcal mol^{-1} rad^{-2}, respectively.

Thermal Denaturation. The thermal denaturation was followed by 1D NMR obtained on samples in ^2H_2O previously used for exchange experiments. The temperature within the NMR samples was calibrated with ethylene glycol. Chemical shifts for fully unfolded species δ_u could not be attained experimentally and were taken as random coil chemical shifts of the corresponding protons (*33*−*35*). Since we could not precisely determine chemical shifts for fully folded species δ_F, these were obtained from fitting experimental $\delta(T)$ to a simple two-state unfolding mechanism (*36*) using Kaleidagraph (Synergy Software):

$$\delta(T) = \alpha\delta_F + (1 - \alpha)\delta_u$$

where $\alpha = 1/(1 + e^{-\Delta G/RT})$.

Then the two-state equilibrium constant for unfolding,

$$K_U^{thermal} = f_U/(1 - f_U) = [\delta_F - \delta(T)]/[\delta(T) - \delta_U]$$

and

$$\Delta G_U^{thermal} = -RT \ln K_U^{thermal}$$

was determined at each experimental temperature (f_U, fraction unfolded).

The $\Delta H_U^{thermal}$, for the reversible unfolding of the peptides, was obtained from the van't Hoff formalism:

$$\partial[\ln(K_U^{thermal})]/\partial\left(\frac{1}{T}\right) = -\Delta H_U^{thermal}/R$$

by linear fit of $\ln(K_U^{thermal})$ versus $1/T$. $\Delta S_U^{thermal}$ and T_m for reversible thermal unfolding of the peptides were calculated by linear fitting of $\Delta G_U^{thermal}$ versus T (*37*).

The statistical error on experimental chemical shifts was estimated to ±0.01 ppm. To obtain a rough estimate of the corresponding error for the calculated thermodynamics parameters, the above calculations were repeated 100 times with chemical shifts randomly picked in the range of $x \pm 0.01$ ppm, where x is the experimentally determined value. From the resulting distributions of parameters, mean values and associated standard deviations were calculated and are reported in Table 2.

RESULTS AND DISCUSSION

Design of Peptides Min-21 and Min-23

Two arguments were considered to show that the elementary CSB motif only contains two disulfide bridges: (i) the structural superposition of various compounds containing the motif indicating that only two disulfide bridges are remarkably well-conserved, with the other disulfide bridges not being structurally conserved, and (ii) the observation of a stable two-disulfide intermediate in the folding of EETI II (*24*). Our design of the minimal peptide that would fold as a CSB motif thus started with EETI II, which is moreover one of the shortest peptides known to include the CSB motif. First, the disulfide bridge between cysteines 2 and 19 must be removed as it is not part of the CSB motif (see above). To simplify comparisons between peptides, all residue numbering will now refer to the parent peptide EETI II as shown in Figure 2. Second, the first five residues, including cysteine 2, are removed as these are not part of the CSB motif and bear the inhibitory site of EETI II that is no longer needed. The CSB motif starts at residue Met^7 in EETI II (the first residue of the first β-strand); thus, we could have removed Leu^6. However, the nuclear magnetic resonance spectroscopy study of EETI II has shown that a hydrophobic cluster is formed by interaction of Leu^6 with Phe^{26} which may be important for the stability of the molecule. We thus chose not to remove this interaction and started the shortened peptide at Leu^6. Third, cysteine 19, which bridged with cysteine 2 and has now lost its pairing partner, is replaced by a serine. The replacement of a cysteine by a serine was already used in several EETI II analogues (*38*, *39*). All these

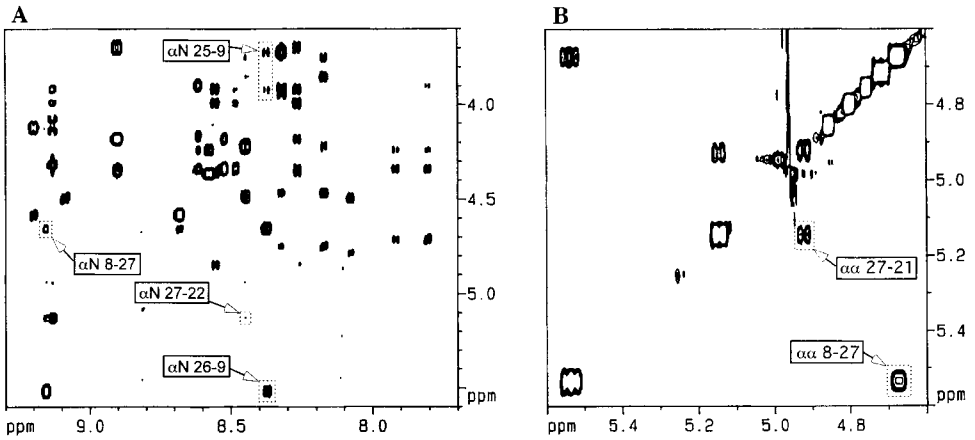

FIGURE 3: Portions of the 2D NOESY spectrum of Min-23 at 12 °C and pH 2.7 showing the NOEs between protons on adjacent β-strands: (A) NOEs between amide and α-protons and (B) NOEs between α-protons.

considerations resulted in a 23-residue long peptide that will be called Min-23 (Figure 2). Nevertheless, comparison of the 3D structure of EETI II and ω-conotoxin suggests that the β-turn from residue 16 to 19 may be shortened as this region is two residues shorter in ω-conotoxin (Figure 2). We thus also considered a still shorter peptide called Min-21 (Figure 2). In this peptide, the two central residues in the region of residues 16−19, i.e., residues 17 and 18, have been removed. The new turn is now made up of residues Cys[15], Leu[16], Cys[19], and Val[20]. In ω-conotoxin, the corresponding residues are Cys, Cys, Arg, and Ser. Of course, we do not want any additional cysteine residue except Cys[15]. Therefore, we can keep Leu[16], but we must replace Cys[19]. We could have replaced Cys[19] by a serine as in Min-23, or by an arginine as in ω-conotoxin. However, none of these mutations appear to be necessary, and we instead chose to replace Cys[19] with a glycine, a residue commonly found in position 3 of β-turns and actually present at position 3 of the corresponding β-turn in EETI II and Min-23 (i.e., Gly[18]). Finally, to avoid possible sensitivity to oxidation of Met[7], this residue was replaced by the more stable isosteric residue norleucine in the two peptides.

Solution Structure of Peptides Min-21 and Min-23

NMR Experiments. NMR experiments show that Min-23 and Min-21 share the same overall fold with EETI II. Complete ^{1}H chemical shift assignments are provided in the Supporting Information. The α-proton chemical shifts, $^3J_{HN-H\alpha}$ coupling constants, and NOEs measured on Min-23 are quite similar to those obtained on EETI II. All the expected NOEs between the three antiparallel β-strands are observed (Figure 3), except two of them which cannot be detected. In Min-23, the resonance of Hα[21] being under the residual water signal, the NOE Hα[21]−HN[28] was not observed as well as the NOE between HN[7] and HN[27], which have very close chemical shifts. Nevertheless, several NOEs were detected between protons of residues 7 and 27. In the 3_{10}-helix (residues 11−15) and in the β-turn of residues 16−19, the NOE patterns are the same for the two peptides.

With regard to the tertiary NOEs, examination of Figure 4 shows that most of them are common to Min-23 and EETI II. Nevertheless, several differences are noticeable that could reveal either small conformational changes or higher flexibility in Min-23 such as the backbone−backbone contacts

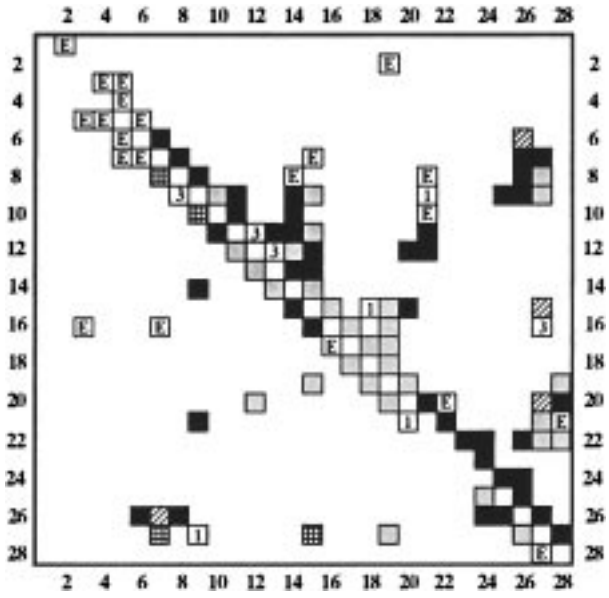

FIGURE 4: Comparison of the NOEs observed for EETI II, Min-23, and Min-21. The NOEs involving at least one backbone proton are shown above the diagonal except for d_{NN} NOEs which are shown below the diagonal together with side chain−side chain NOEs: (black boxes) NOEs detected in the three peptides, (gray boxes) NOEs observed in EETI II and Min-23, (hatched boxes) NOEs observed in EETI II and Min-21, and (grid boxes) NOEs observed in Min-23 and Min-21. NOEs observed in one peptide only are labeled E, 3, and 1 for EETI II, Min-23, and Min-21, respectively.

between Arg[8] and Asp[14], between Cys[21] and Arg[8], and between Cys[21] and Lys[10], which are not observed in Min-23.

With regard to Min-21, although secondary and tertiary NOEs common to Min-23 and EETI II were observed (Figure 4), they are less numerous. Several amide protons gave broad resonances in the 1D spectrum. The α-proton chemical shifts showed large differences compared to those of EETI II and Min-23 (up to 0.35 ppm). All these elements are in favor of a more flexible conformation for Min-21 as compared with EETI II and Min-23. This flexibility is confirmed by the exchange rate measurements of backbone amide protons (see below) and by the fact that only three stereospecific assignments of the β-protons (*40*) could be achieved for Min-21 instead of nine for Min-23. Similarly, $^3J_{HN-H\alpha}$ coupling constant values allowed determination of only three φ

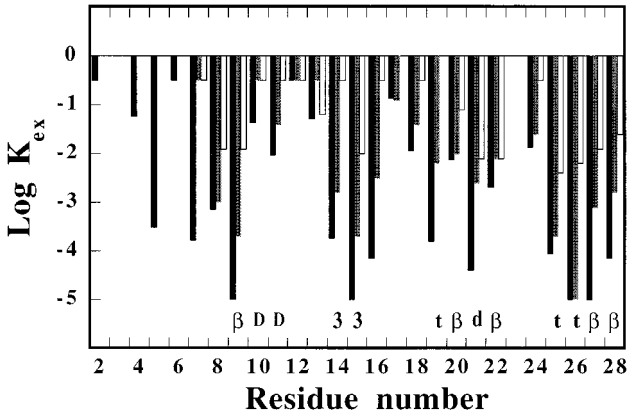

FIGURE 5: Proton−deuteron exchange rates log(K_{ex}) of the backbone amide protons determined for the three peptides: (black bars) EETI II, (gray bars) Min-23, and (white bars) Min-21. Values for amide protons which exchange very fast and were not observed on the first 1D spectrum were set at −0.5. Values for amide protons whose intensity did not change after a 48 h exchange were set at −5.0. Aspartic acid side chains involved in H-bonds with amide protons (d being Asp[12] and D being Asp[14]) as well as H-bonded amide protons involved in secondary structures (t being turn, β being β-sheet, and 3 being 3_{10} helix) in EETI II are denoted at the bottom.

dihedral angles for Min-21 instead of 10 for Min-23 (see the Supporting Information).

Information about the stability of the molecules can be obtained from amide proton exchange experiments. Values obtained for EETI II and the Min-23 and Min-21 peptides are shown in Figure 5. It is usually assumed that amide protons in H-bonds can exchange with the solvent only when they are transiently exposed through a so-called "open" conformation. An increase in the exchange kinetics of an analogue may then result from a higher intrinsic solvent accessibility, i.e., through conformational change, or from a modification of the equilibrium between the open and the closed conformation as a consequence of increased local and/or global dynamics of the protein. Slowly exchanging amide protons in EETI II are essentially those involved in backbone−backbone or backbone−side chain H-bonds (Figure 5, black bars). All corresponding protons in Min-23 exhibit faster exchange kinetics probably indicative of overall lower stability. The changes appear to be of similar magnitude in the β-sheet area (amides 9, 20, 22, 27, and 28) and in the helix (amides 14 and 15). The turn of residues 22−25 (amides 25 and 26) seems to be only marginally affected, whereas the turn of residues 16−19 (amide 19) is more strongly affected. This is not unexpected since the disulfide bridge between Cys[2] and Cys[19], connecting the N-terminal segment to the turn of residues 16−19 in EETI II, has been removed in Min-23, probably relaxing some constraints on the β-turn of residues 16−19. H-bonds between amide protons of residues 10, 11, and 21 with aspartic side chains also appear to be weaker in Min-23.

In Min-21, all exchanges are still much faster. The β-turn of residues 16−19 does not exist any more and cannot be compared. The helix seems to be more destabilized than the β-sheet with amide 14 now exchanging very fast. HN[10] and HN[11] that make H-bonds with the Asp[14] side chain in EETI II and Min-23 now also exchange very fast. Here again, the β-turn of residues 22−25 is less affected and amides 25 and 26 are now the most slowly exchanging ones.

From these results, it is clear that removing five residues and one disulfide bridge from the sequence of native EETI II leads to a slightly less stable peptide that nevertheless retains all the main structural features of the native protein. Removing two more residues lowers the stability even more with the loss of a few structural characteristics, although again, the overall fold is conserved. Therefore, the CSB structural motif alone is less stable than the parent native protein that contains one supplementary disulfide bridge. Nevertheless, the CSB motif still appears to be very stable and able to fold by itself.

Structure Calculations. The three-dimensional structure of the peptides Min-21 and Min-23 were determined from NMR spectroscopy using the same strategy previously used for structural studies of native EETI II and of analogues (*14*, *15*, *24*, *38*, *39*). The NMR study led to 60 sequential and 93 medium- and long-range NOEs for Min-23 (44 and 51, respectively, for Min-21). Ten ϕ angles were determined from the $^3J_{HN-H\alpha}$ coupling constant for Min-23 (three for Min-21). Stereospecific assignment of the Hβ protons was achieved for nine residues in Min-23 and three residues in Min-21. The NMR data were converted into distance and angle constraints as usual. The dihedral constraints that were used are available as Supporting Information, as well as the statistics for constraint violations and for molecular mechanics energies. The program DYANA (*28*) was used to compute 3D conformations that are compatible with the constraints using the torsion angle dynamics method. Using AMBER 5.0 (*29*), the resulting models were further refined using a molecular dynamics simulated annealing protocol. As the cysteine connectivities were unknown, we used the same strategy that was previously used for native EETI II; i.e., structure calculations were performed with the three different possible disulfide bridges (*14*). As previously discussed for the native protein, the close proximity of the cysteine residues results in different bridges being accessible with only very small structural modifications. Consequently, the distance violations were only weakly affected by modification of the connectivity, although for both peptides the sum of the violations was lower for native connectivities. Fortunately, in both peptides, we were able to unambiguously determine the χ_1 rotamer for at least two cysteines from coupling constants and NOEs between HN, Hα, Hβ2, and Hβ3 (*40*). In contrast to interatomic distances, the cysteine χ_1 dihedrals are strongly affected by the cysteine connectivity, and it now follows from the dihedral violations that only native connectivities are consistent with the NMR data. This conclusion is moreover fully supported by the molecular mechanics and constraint energies. Solution structures of peptides Min-21 and Min-23 superimposed onto native EETI II are displayed in Figure 6. The global rms deviation between structures is reported in Table 1, and the local rms deviation along the sequence is displayed in Figure 7.

The structure of Min-23 is reasonably well-resolved with a low global backbone rms deviation (0.29 ± 0.11 Å for superimposition of the N, Cα, and C atoms of residues 7−27). Leu[6], which is the N-terminal residue in the shortened peptides and is not involved in any secondary structure, exhibits a larger rms deviation value of 1.2 Å. Residues 7, 8, and 28 of the N- and C-termini participate in the triple-stranded β-sheet and exhibit only slightly higher values than average (up to ≈0.5 Å). It is interesting to note that, besides

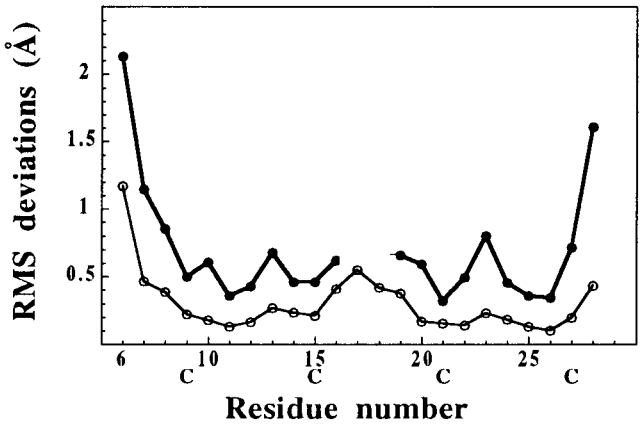

FIGURE 6: Average rms deviation between calculated structures. The 20 calculated structures for each peptide were superimposed pairwise for the backbone atoms of residues 7−27. The average rms deviations are plotted along the sequence as black circles (Min-21) and white circles (Min-23). The position of the cysteines is denoted by the letter C at the bottom.

Table 1: rms Deviations and Disulfide Bridge Conformations of Computed Peptide Models

	rms Deviations[a,b] (Å) Min-23	Min-21
backbone	0.3 (0.1)	0.6 (0.2)
heavy atoms	1.3 (0.3)	1.7 (0.3)

	Disulfide Bridges[a]		
χ_1	EETI II	Min-23	Min-21
Cys^9	50.7	66.5 (2.4)	74.6 (5.0)
Cys^{21}	−173.8	−173.1 (1.9)	165.5 (4.6)
Cys^{15}	−58.0	−51.0 (3.0)	−163.8 (6.5)
Cys^{27}	−63.1	−64.0 (1.6)	179.3 (8.8)

[a] Mean values and standard deviations in parentheses obtained for the 20 calculated structures. [b] rms deviations are for the superimposition of backbone or heavy atoms of residues 7−27.

Leu^6, the part of the peptide with the larger fluctuations is the β-turn of residues 16−19, a result highly consistent with the amide exchange experiments.

Clearly, the structure of Min-21 is less well-defined than that of Min-23, with a larger global backbone rms deviation (0.62 ± 0.20 Å for the superimposition of the N, Cα, and C atoms of residues 7−27). The local rms deviations are always approximately twice as large for Min-21 as for Min-23. This was not expected a priori since shortening the turn of residues 16−19 might have introduced additional stereochemical constraints in a small peptide already constrained by two disulfide bridges, thus limiting the available conformational space. This is not the case, however, and NMR data clearly indicate that Min-21 possesses a less well-defined conformation than Min-23 (line broadening, exchange experiments, number of possible stereospecific assignments, and rms deviations between calculated structures).

Comparison of Min-23 with native EETI II (Figure 6) reveals very good structure conservation, showing that the CSB motif is barely affected by removing the additional residues present in the native protein. Almost all H-bonds that define the elements of secondary structure in EETI II are conserved in Min-23: β-sheet, $O^7\cdots HN^{27}$, $O^{25}\cdots HN^9$, $O^{20}\cdots HN^{28}$, and $O^{26}\cdots N^{22}$; 3_{10}-helix, $O^{11}\cdots HN^{14}$ and $O^{12}\cdots HN^{15}$; and β-turns, $O^{16}\cdots HN^{19}$ and $O^{22}\cdots HN^{25}$,HN^{26}.

Also, two H-bonds between carboxylic acid side chains and backbone atoms present in EETI II are conserved in all Min-23 calculated structures: $Asp^{14}\cdots HN^{10}$,HN^{11} and $Asp^{12}\cdots HN^{21}$. Note however that the last H-bond of the β-sheet ($O^{28}\cdots HN^{20}$) seen in EETI II is disrupted in Min-23 and O^{28} now H-bonds with the side chain of Ser^{19} (a residue that replaces Cys^{19} of EETI II). The $O^{28}\cdots HN^{20}$ H-bond is also absent in many Min-21 structures (Figure 6). In this case, however, O^{28} cannot H-bond with side chain of residue 19 which is now a glycine (it is a serine in Min-23), resulting in a larger rms deviation value for Gly^{28} (Figure 7). The replacement of a backbone−backbone H-bond in EETI II with a backbone−side chain H-bond in Min-23 probably contributes to the reduced stability of Min-23. Similarly, the complete loss of this H-bond in Min-21 is consistent with the increased flexibility of Min-21. Moreover, in Min-21, and in agreement with the amide exchange data, the H-bonds with aspartic acid side chains are not fully conserved. The $Asp^{12}\cdots HN^{21}$ H-bond is present in only seven structures out of 20, and alternative H-bonding of Asp^{12} with the amide of Gly^{19}, which belongs to the modified region between Min-21 and Min-23, is also observed. Even more, the $Asp^{14}\cdots HN^{10}$,HN^{11} H-bond is observed in only one structure. This simply suggests that there is no particular H-bond involving aspartic acid side chains, which is very strong in Min-21. It should be kept in mind that this does not provide any information about the persistence of these H-bonds in solution since calculations were carried out in vacuo, and there were no competing solvent molecules. Indeed, stereospecific assignment could be achieved for aspartic acids in Min-23 but not in Min-21, and this is certainly related to a larger conformational flexibility of these residues in Min-21, as also indicated by line broadening, amide proton exchange experiments, and larger rms deviations between calculated structures.

χ_1 angles for cysteines in the calculated structures are listed in Table 1. Min-23 exhibited disulfide bridge conformations very similar to those in native EETI II. For this peptide, Hβ protons of all four cysteine residues could be stereospecifically assigned and corresponding rotamers were determined to be identical to those in EETI II. Rotamers of only two cysteine residues could be determined for Min-21, i.e., for Cys^9 and Cys^{15}. The Cys^9 rotamer was the same as in Min-23 and EETI II, and the corresponding Cys^9−Cys^{21} disulfide bridge exhibited a conformation similar to that of EETII II and Min-23. The Cys^{15} rotamer, however, was different from both EETI II and Min-23, and the Cys^{15}−Cys^{27} disulfide bridge exhibited rather well-defined conformations different from those in EETI II and Min-23 (Table 1). This modification may be a result of the shortening of the turn of residues 16−19 that induces conformational modification of the close Cys^{15}. Indeed, Leu^{16} in Min-21 is significantly displaced from the position it occupies in EETI II and Min-23 and now points toward the solvent (Figure 6). Accordingly, the contact between Leu^{16} and Cys^{27}, present in Min-23, was no longer detected in Min-21.

Thermal Stability

To more carefully evaluate the stability of the CSB motif, EETI II, Min-23, and Min-21 were submitted to thermal unfolding experiments. Thermal unfolding of proteins is traditionally assessed using circular dichroism, ultraviolet,

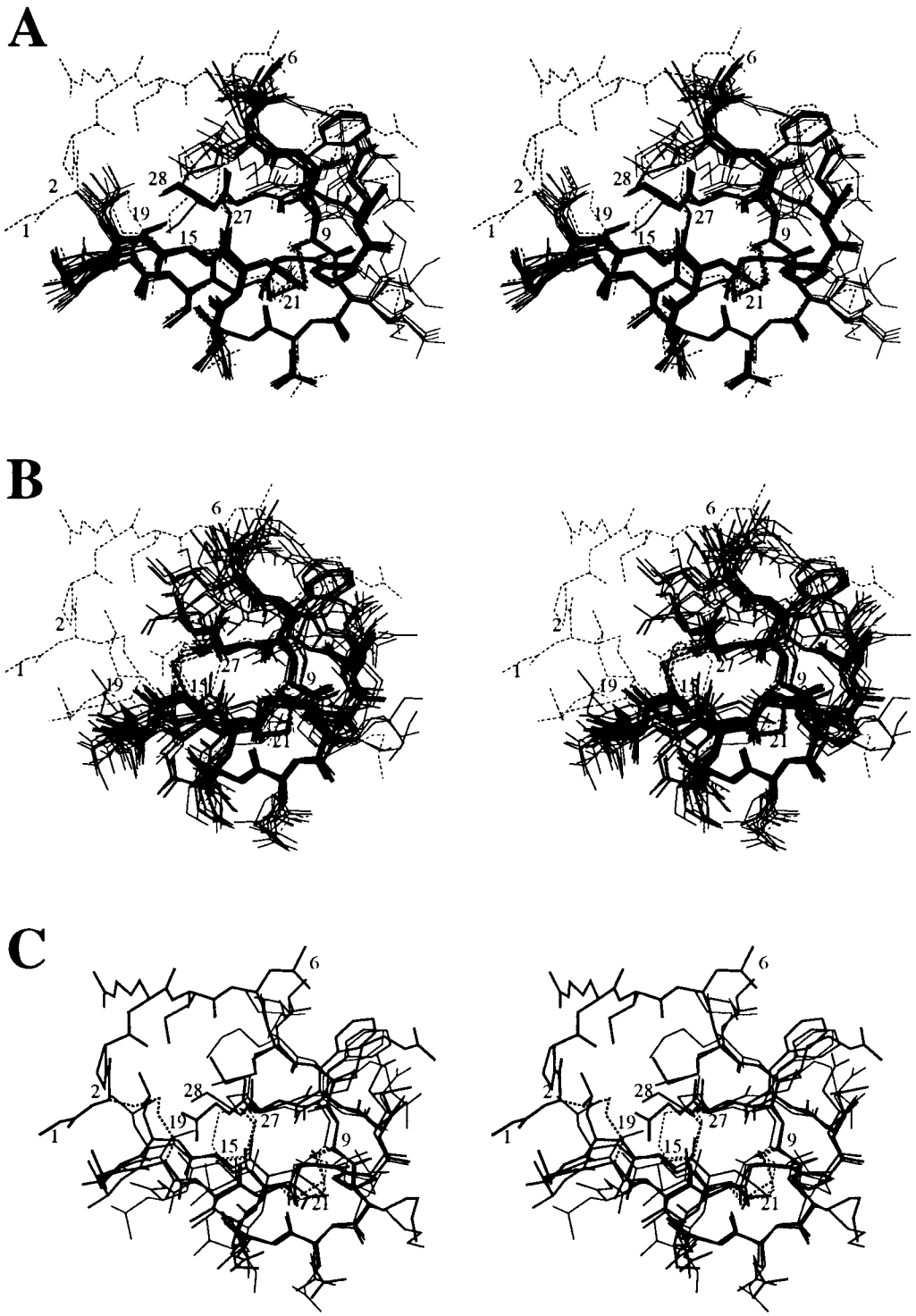

FIGURE 7: Stereoviews of the computed solution structures of peptides (A) Min-23 and (B) Min-21. Fifteen calculated structures are displayed for each peptide as thick lines (backbone) and thin lines (side chains). The disulfide bridges as well as the native inhibitor EETI II are depicted as thin dashed lines. (C) Superimposition of the solution structures closest to the average conformations of Min-21 (thin lines) and Min-23 (medium lines) and of EETI II (thick lines). All structures were superimposed for backbone atoms of residues 7−27. The cysteines and the N- and C-termini are numbered.

or fluorescence spectroscopy, or studied by differential scanning calorimetry. Unfortunately, wild-type EETI II and the shortened analogues do not possess good ultraviolet or fluorescent probes (there is only one phenylalanine in the sequences). Moreover, the circular dichroism spectra of these compounds are difficult to analyze, possibly because of the limited amount of standard secondary structures and the contribution of the three disulfide bridges. On the other hand, NMR spectroscopy has been used many times in recent years to study thermal unfolding by monitoring the change in chemical shifts as a function of temperature (*36*, *41*, *42*). It has been shown in one case that using different approaches gives superimposable results (*41*). One advantage of using NMR is that specific information may be obtained for different parts of the protein. The native protein and the Min-21 and Min-23 peptides have T_m values that are too high for attaining fully unfolded species under conditions accessible to NMR experiments in H_2O. Therefore, proton chemical

shift values for fully unfolded species were assimilated to random coil chemical shift values determined for small peptides (*33*−*35*). The experimental data and the theoretical values for the unfolded species were fitted to a simple two-state process (*36*), allowing determination of the theoretical chemical shift value for the fully folded species. From this, the fraction of protein in the unfolded conformation at each experimental temperature was calculated, allowing evaluation of the equilibrium constant K for the equilibrium between folded and unfolded forms and the associated $\Delta G_U^{thermal}$. A van't Hoff plot of ln K as a function of $1/T$ exhibited an almost linear relationship, indicating that heat capacity does not vary significantly during experimental unfolding, and $\Delta H_U^{thermal}$ was obtained from a linear fit. The heat capacity variation usually observed during protein unfolding has been ascribed to exposure of a much larger hydrophobic surface in the unfolded form (*43*). Thus, two effects may be invoked to explain the almost constant heat capacity during Min-21 and Min-23 unfolding: (i) the small size of the protein precludes burying of a large hydrophobic surface area in the folded form, and (ii) the disulfide bridges prevent the unfolded form from acquiring fully accessible conformations. Then, from a plot of $\Delta G_U^{thermal}$ as a function of T, T_m was taken as the temperature at which $\Delta G_U^{thermal} = 0$ and $\Delta S_U^{thermal}$ was taken as the slope of $\Delta G_U^{thermal}$ versus T at T_m (*37*).

The unfolding curves for several protons are displayed in Figure 8, and thermodynamic parameters are listed in Table 2. Only one comparison could be made between Min-23 and native EETI II for the β-protons of Cys^{21}. The other EETI II protons that could be monitored during temperature variation exhibited no significant chemical shift modification. Even for the Cys^{21} β-protons, EETI II unfolding remained very limited (fraction unfolded < 0.2) and only allowed a very rough estimation of the thermodynamical data. The approximate difference in T_m between Min-23 and EETI II is about 40° which might be reasonable, but the calculated $\Delta\Delta G_U^{thermal}$ is only 0.6 kcal mol^{-1} at 17 °C, and is probably underestimated. Indeed, all observations indicate that Min-23 is less stable than EETI II: faster exchange of all amide protons involved in H-bonds and larger thermal unfolding. Nevertheless, the data in Table 2 clearly indicate that Min-23 retains strong thermal stability. Not unexpectedly, side chain protons exhibit lower T_m values (85−96 °C) than backbone protons (102−112 °C). The highest T_m values are observed for Hα protons of Gly^{25}. The Hα proton of Phe^{26} exhibits a larger $\Delta G_U^{thermal}$ (3.4 kcal mol^{-1}), whereas other protons exhibit $\Delta G_U^{thermal}$ values between 1.9 and 2.5 kcal mol^{-1}.

Min-21 exhibits a still lower stability with a T_m near 60 °C. As in Min-23, the highest T_m values are observed for Hα protons of Gly^{25} (82 and 92 °C). The T_m difference between Min-23 and Min-21 is in the range of 20−40 °C. $\Delta G_U^{thermal}$ values for Min-21 ($\Delta G_U^{thermal} \approx 1.2-1.5$ kcal mol^{-1}) are quite constant for the protons that were studied and significantly lower than that observed for Min-23. The calculated $\Delta\Delta G_U^{thermal}$ between the two peptides is close to 1 kcal mol^{-1} except for the Hα of Phe^{26} for which a value that is twice as large is obtained.

In Min-23, the Hα of Phe^{26} exhibits a higher T_m than the side chain protons (Leu^6 and Phe^{26}), and among the side chains, Leu^6, which is the first residue and which is not involved in secondary structure, has the lowest T_m. These results do make sense and are in accordance with general concepts on protein structure. In Min-21, all protons exhibit similar variations, except the Hα of Phe^{26} which now behaves in the same manner as the side chain aromatic protons of Phe^{26} (Table 2 and Figure 8). This may indicate some instability in the backbone near Phe^{26}, although the previous Gly^{25} residue did not exhibit such a behavior. The instability of Phe^{26} might rather be related to its proximity to Cys^{27}, which is involved in a disulfide bridge, the conformation of which was modified between Min-23 and Min-21.

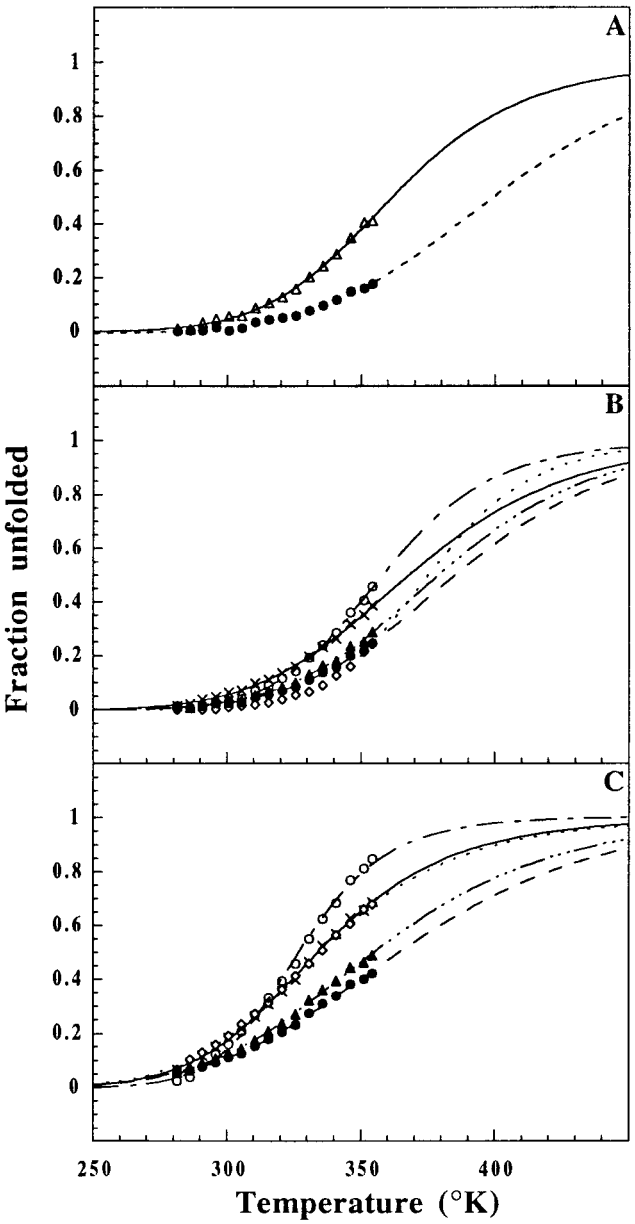

FIGURE 8: Thermal unfolding curves. The fraction unfolded calculated from the chemical shift (see Materials and Methods) is plotted as a function of temperature. (A) β-Proton of Cys^{21} in EETI II (●) and Min-23 (△). (B) Min-23 peptide. (C) Min-21 peptide. Proton identification is as follows: Leu^6 Hδ (○), Gly^{25} Hα2 (▲), Gly^{25} Hα3 (●), Phe^{26} H2,H6 (×), and Phe^{26} Hα (◇).

CONCLUSION

In this paper, we have described the design, the structure, and the stability of two peptides, Min-21 and Min-23, that

Table 2: Thermodynamic Parameters for Peptide Thermal Unfolding

proton	compound	$\Delta H_U^{thermal\ a,b}$	$T_m^{a,c}$	$\Delta S_U^{thermal\ a,d}$	$\Delta G_U^{thermal\ a,b}$	$\Delta\Delta G_U^{thermal\ a,b}$
Cys^{21} Hβ	EETI II	10[h]	127	25[h]	2.7[i]	
	Min-23	11	89	29	2.1	0.6[e]
Leu^{6} Hδ	Min-23	13[i]	85	36[i]	2.5[i]	
	Min-21	14	54	42	1.5	1.0[f]
Gly^{25} Hα2[g]	Min-23	11[h]	106	28[h]	2.5[h]	
	Min-21	8	82	22	1.4	1.1[f]
Phe^{26} H2,H6	Min-23	9	96	25	1.9	
	Min-21	9	62	27	1.2	0.7[f]
Phe^{26} Hα	Min-23	15[i]	102	40[i]	3.4[i]	
	Min-21	9	62	26	1.2	2.2[f]

[a] Mean values, and standard deviations, obtained from multiple calculations as described in Materials and Methods. Standard deviations are ±1−15%. [b] Values are in kilocalories per mole. [c] Values are in degrees Celsius. [d] Values are in kilocalories per mole per kelvin. [e] $\Delta\Delta G_U^{thermal} = \Delta G_U^{thermal}$(EETI II) − $\Delta G_U^{thermal}$(Min-23). [f] $\Delta\Delta G_U^{thermal} = \Delta G_U^{thermal}$(Min-23) − $\Delta G_U^{thermal}$(Min-21). [g] Values for Gly^{25} Hα3 are very similar. [h] Standard deviations are ±30−45%. [i] Standard deviations are ±15−30%.

are believed to be the shortest ones to contain the widespread CSB elementary structural motif. The two peptides contain only two disulfide bridges, whereas all native proteins built on this motif contain at least one supplementary disulfide bridge. Nevertheless, both peptides were shown to fold correctly in a native-like fashion, thus lending support to the initial hypothesis that the elementary motif only contains two disulfide bridges and is an autonomous folding unit.

Min-23 exhibits a well-defined conformation, very similar to the structure of the native parent inhibitor EETI II. Although Min-23 is less stable than EETI II, it nevertheless retains high thermal stability, with a mean T_m of almost 100 °C (Table 2). Min-21 is only two residues shorter, but its conformation is clearly much less well defined. The difference in stability between Min-23 and Min-21 is about 1 kcal mol^{-1}. At the moment, this difference cannot be explained in detail. The shortening of the turn of residues 16−19 resulted in a modified conformation of the disulfide bridge of residues 15−27 and in loosened H-bonds of the Asp^{12} and Asp^{14} side chains with backbone amides. However, this turn modification was designed on the basis of the structure of ω-conotoxin that seems to accommodate the short turn without apparent structural constraints. It is worth noting that the third disulfide bridges in native EETI II (Cys^2−Cys^{19}) and in native conotoxin (Cys^2−Cys^{16}) are differently located with respect to the turn of residues 16−19 and might play a very different role in stabilizing the native proteins. Therefore, it is possible that removing these third disulfide bridges in Min-21 and Min-23 leads to different and unexpected results for the two peptides. Analysis of the structure of ω-conotoxin also indicates that, in contrast to Min-21 and Min-23, the segment between Cys^9 and Cys^{15} contains no 3_{10}-helix and is one residue longer. This may provide Cys^{15} with a sufficient degree of freedom that it forms a disulfide bridge from residue 15 to 27 with a conformation similar to the one in EETI II, despite a segment that is two residues shorter between cysteines 15 and 19. In Min-21, the loss of freedom of Cys^{15} due to the short segment of residues 15−19 is not offset by relaxing residues 9−15, probably forcing the disulfide bridge from residue 15 to 27 to adopt a different conformation. This modification is accompanied by a significant displacement of residues 16 and 19 (Figure 6). It is also possible that the constraints on Cys^{27} destabilize the triple-stranded β-sheet near Cys^{27} and are responsible for the particular behavior of the Phe^{26} Hα proton in the thermal unfolding experiments with Min-21. It therefore seems that the sequence of Min-21 is not optimal for the CSB fold, although more theoretical and experimental studies remain to be done on these peptides and on analogues to fully understand the reasons for the reduced stability of Min-21. Nevertheless, the study of Min-21 already affords one interesting conclusion concerning the length of the segments connecting cysteines in the CSB motif. The alignment in Figure 2 and other alignments not shown suggest that these segments can vary largely in length and that the sequences C-x_5-C-x_4-C and C-x_6-C-x_2-C (where x is any amino acid) are among the shortest possible connections between the first and third cysteines in the CSB motif. However, the reduced stability of Min-21 indicates that these connections cannot be combined to give C-x_5-C-x_2-C without a significant loss of stability.

It is worth noting that, in both peptides, the turn of residues 22−25 exhibited peculiar properties. First, the amide proton exchanges remained slow while other regions were more affected when compared with the native inhibitor EETI II. Second, the calculated T_m values of the Gly^{25} Hα protons are the highest observed in each peptide. This might well be related to the high β-turn propensity of this sequence and to its possible involvement in a folding nucleation site (*39*, *44*).

The main goal of this study was to design a short peptide with the CSB motif that is stable, easy to fold, and devoid of any active site. Min-23 appears to be such a peptide and therefore constitutes a very good starting building block for engineering new bioactive compounds by grafting active or recognition sites. Min-21 is less stable but retains the essential structural features and might be useful if a higher flexibility is desired. It is hoped that the characterization of the elementary CSB motif described in this paper will help in the elucidation of relationships between sequences and structures of small disulfide-rich proteins and will provide a new and interesting basis for future design projects.

ACKNOWLEDGMENT

We thank S. L. Salhi for English revisions of the manuscript.

SUPPORTING INFORMATION AVAILABLE

^{1}H chemical shift assignments of EETI II, Min-23, and Min-21, data on distance and angle constraints used for structure calculations, and statistics on constraint violations

and molecular mechanics energies of the calculated structures. This material is available free of charge via the Internet at http://pubs.acs.org.

REFERENCES

1. Nygren, P., and Uhlen, M. (1997) *Curr. Opin. Struct. Biol. 7*, 463−469.
2. Cunningham, B. C., and Wells, J. A. (1997) *Curr. Opin. Struct. Biol. 7*, 457−462.
3. Vita, C., Roumestand, C., Toma, F., and Menez, A. (1995) *Proc. Natl. Acad. Sci. U.S.A. 92*, 6404−6408.
4. Vita, C. (1997) *Curr. Opin. Biotechnol. 8*, 429−434.
5. Tamaoki, H., Miura, R., Kusunoki, M., Kyogoku, Y., Kobayashi, Y., and Moroder, L. (1998) *Protein Eng. 11*, 649−659.
6. Orengo, C. A., Flores, T. P., Taylor, W. R., and Thornton, J. M. (1993) *Protein Eng. 6*, 485−500.
7. Lesk, A. M. (1995) *J. Mol. Graphics 13*, 159−164.
8. Wang, Z.-X. (1998) *Protein Eng. 11*, 621−626.
9. Tamaoki, H., Kobayashi, Y., Nishimura, S., Ohkubo, T., Kyogoku, Y., Kumagaye, S., Kimura, T., and Sakakibara, S. (1991) *Protein Eng. 4*, 509−518.
10. Pagel, M., and Wemmer, D. (1994) *Proteins 18*, 205−215.
11. Pallaghy, P. K., Nielsen, K. J., Craik, D. J., and Norton, R. S. (1994) *Protein Sci. 3*, 1833−1839.
12. Norton, R. S., and Pallaghy, P. K. (1998) *Toxicon 36*, 1573−1583.
13. Narasimhan, L., Singh, J., Humblet, C., Guruprasad, K., and Blundell, T. (1994) *Nat. Struct. Biol. 1*, 850−852.
14. Heitz, A., Chiche, L., Le-Nguyen, D., and Castro, B. (1989) *Biochemistry 28*, 2392−2398.
15. Chiche, L., Heitz, A., Padilla, A., Le-Nguyen, D., and Castro, B. (1993) *Protein Eng. 6*, 675−682.
16. Kim, J. I., Konishi, S., Iwai, H., Kohno, T., Gouda, H., Shimada, I., Sato, K., and Arata, Y. (1995) *J. Mol. Biol. 250*, 659−671.
17. Pallaghy, P. K., Duggan, B. M., Pennington, M. W., and Norton, R. S. (1993) *J. Mol. Biol. 234*, 405−420.
18. Davis, J. H., Bradley, E. K., Miljanich, G. P., Nadasdi, L., Ramachandran, J., and Basus, V. J. (1993) *Biochemistry 32*, 7396−7405.
19. Vervoort, J., van den Hooven, H. W., Berg, A., Vossen, P., Vogelsang, R., Joosten, M. H., and de Wit, P. J. (1997) *FEBS Lett. 404*, 153−158.
20. Arai, K., Ishima, R., Morikawa, S., Miyasaka, A., Imoto, T., Yoshimura, S., Aimoto, S., and Akasaka, K. (1995) *J. Biomol. NMR 5*, 297−305.
21. Qu, Y., Liang, S., Ding, J., Liu, X., Zhang, R., and Gu, X. (1997) *J. Protein Chem. 16*, 565−574.
22. Saether, O., Craik, D. J., Campbell, I. D., Sletten, K., Juul, J., and Norman, D. G. (1995) *Biochemistry 34*, 4147−4158.
23. Daly, N. L., Koltay, A., Gustafson, K. R., Boyd, M. R., Casas-Finet, J. R., and Craik, D. J. (1999) *J. Mol. Biol. 285*, 333−345.
24. Le-Nguyen, D., Heitz, A., Chiche, L., El Hajji, M., and Castro, B. (1993) *Protein Sci. 2*, 165−174.
25. Harrison, P. M., and Sternberg, M. J. E. (1996) *J. Mol. Biol. 264*, 603−623.
26. Cornet, B., Bonmatin, J. M., Hetru, C., Hoffmann, J. A., Ptak, M., and Vovelle, F. (1995) *Structure 3*, 435−448.
27. Tam, J. P., and Shen, Z. Y. (1992) *Int. J. Pept. Protein Res. 39*, 464−471.
28. Güntert, P., Mumenthaler, C., and Wüthrich, K. (1997) *J. Mol. Biol. 273*, 283−298.
29. Case, D. A., Pearlman, D. A., Caldwell, J. W., Cheatham, T. E., Ross, W. S., Simmerling, C. L., Darden, T. A., Merz, K. M., Stanton, R. V., Cheng, A. L., Vincent, M., Crowley, M., Ferguson, D. M., Radmer, R. J., Seibel, G. L., Singh, U. C., Weiner, P. K., and Kollman, P. A. (1997) *AMBER 5*, University of California, San Francisco, CA.
30. Cornell, W. D., Cieplak, P., Bayly, C. I., Gould, I. R., Merz, K. M., Jr., Ferguson, D. M., Spellmeyer, D. C., Fox, T., Caldwell, J. W., and Kollman, P. A. (1995) *J. Am. Chem. Soc. 117*, 5179−5197.
31. Guenot, J. M., and Kollman, P. A. (1992) *Protein Sci. 1*, 1185−1205.
32. van Gunsteren, W. F., and Berendsen, H. J. C. (1977) *Mol. Phys. 34*, 1311−1327.
33. Merutka, G., Dyson, H. J., and Wright, P. E. (1995) *J. Biomol. NMR 5*, 14−24.
34. Wishart, D. S., and Sykes, B. D. (1994) *Methods Enzymol. 239*, 363−392.
35. Bundi, A., and Wüthrich, K. (1979) *Biopolymers 18*, 285−297.
36. Mer, G., Hietter, H., and Lefevre, J. F. (1996) *Nat. Struct. Biol. 3*, 45−53.
37. Pace, C. N., Shirley, B. A., and Thomson, J. A. (1990) in *Protein structure: A practical approach* (Creighton, T. E., Ed.) pp 311−330, Oxford University Press, Oxford, U.K.
38. Heitz, A., Le-Nguyen, D., Castro, B., and Chiche, L. (1997) *Lett. Pept. Sci. 4*, 245−249.
39. Heitz, A., Chiche, L., Le-Nguyen, D., and Castro, B. (1995) *Eur. J. Biochem. 233*, 837−846.
40. Wagner, G., Braun, W., Havel, T., Schaumann, T., Go, N., and Wuthrich, K. (1987) *J. Mol. Biol. 196*, 611−639.
41. Kuhlman, B., Boice, J., Fairman, R., and Raleigh, D. (1998) *Biochemistry 37*, 1025−1032.
42. Holtzer, M. E., Lovett, E. G., d'Avignon, D. A., and Holtzer, A. (1997) *Biophys. J. 73*, 1031−1041.
43. Murphy, K. P., Privalov, P. L., and Gill, S. J. (1990) *Science 247*, 559−561.
44. Rolka, K., Kupryszewski, G., Ragnarsson, U., Otlewski, J., Krokoszynska, I., and Wilusz, T. (1991) in *Peptides 1990* (Giralt, E., and Andreu, D., Eds.) pp 768−771, ESCOM Science Publishers, Leiden, The Netherlands.
45. Kraulis, P. (1991) *J. Appl. Crystallogr. 24*, 946−950.
46. Merritt, E. A., and Bacon, D. J. (1997) *Methods Enzymol. 277*, 505−524.
47. Bernstein, F. C., Koetzle, T. F., Williams, G. J. B., Meyer, E. F., Jr., Brice, M. D., Rodgers, J. R., Kennard, O., Shimanouchi, T., and Tasumi, M. (1977) *J. Mol. Biol. 112*, 535−542.
48. Aumelas, A., Chiche, L., Mahe, E., Le Nguyen, D., Sizun, P., Berthaud, P., and Perly, B. (1991) *Int. J. Pept. Protein Res. 37*, 315−324.
49. Wüthrich, K., Billeter, M., and Braun, W. (1983) *J. Mol. Biol. 169*, 949−961.
50. Wüthrich, K. (1986) *NMR of Proteins and Nucleic Acids*, John Wiley & Sons Inc., New York.

BI990821K